PLANT SCIENCES

In vivo visualization of nitrate dynamics using a genetically encoded fluorescent biosensor

Yen-Ning Chen[1], Heather N. Cartwright[2], Cheng-Hsun Ho[1]*

Nitrate (NO_3^-) uptake and distribution are critical to plant life. Although the upstream regulation of NO_3^- uptake and downstream responses to NO_3^- in a variety of cells have been well studied, it is still not possible to directly visualize the spatial and temporal distribution of NO_3^- with high resolution at the cellular level. Here, we report a nuclear-localized, genetically encoded fluorescent biosensor, which we named NitraMeter3.0, for the quantitative visualization of NO_3^- distribution in *Arabidopsis thaliana*. This biosensor tracked the spatiotemporal distribution of NO_3^- along the primary root axis and disruptions by genetic mutation of transport (low NO_3^- uptake) and assimilation (high NO_3^- accumulation). The developed biosensor effectively monitors NO_3^- concentrations at the cellular level in real time and spatiotemporal changes during the plant life cycle.

INTRODUCTION

The plant root is essential to nutrient uptake. Nitrate (NO_3^-) is a major nitrogen source and is one of the most limiting factors in agricultural production (*1*, *2*). Within the root, NO_3^- levels differ markedly between root cell types (*3*, *4*). Under NO_3^- limitation, plants can optimize morphological and physiological parameters; for example, root growth can be directed toward nutrient deposits in the soil, the root surface area can be locally increased, or the transporter density on the membrane can be altered. Moreover, metabolic conversion, storage, and translocation of nitrogen compounds are modified (*5*, *6*). To adjust these parameters, plants have to monitor both the external and intracellular NO_3^- concentrations to determine NO_3^- acquisition needs by plant roots.

NO_3^- uptake predominantly occurs from the soil/rhizosphere into roots. Once in a root cell, NO_3^- ions can diffuse within the symplasm from cell to cell. NO_3^- ions can serve as an osmotic compound or be assimilated in the root to produce organic nitrogen for cellular growth either locally or be loaded into xylem vessels for transport to the shoot (*7*). NO_3^- uptake, the rate of NO_3^- acquisition by the plant, depends on the surface area of the root; in addition, the environmental factors that affect root growth will also affect NO_3^- capacity. Furthermore, the root system is very plastic, and NO_3^- availability itself strongly affects root development. However, we still do not fully understand the most fundamental aspects of NO_3^- uptake by plant roots, such as which tissue(s) is(are) responsible for NO_3^- uptake, whether NO_3^- uptake is distributed all along the root, and whether NO_3^- uptake is restricted to specific developmental zones. In addition, the exact intercellular path from the outer root layers toward the central stele has only been hypothesized and not experimentally proven. It has proven difficult to track NO_3^- molecules within plant tissue. Some studies have reported NO_3^- detection; however, most of these techniques either lack spatial resolution, e.g., radioactive isotope (*8*, *9*) and the Griess method (*10*), or have limitations to their use, e.g., vibrating electrodes (*11*, *12*), positron-emitting tracer imaging (*13*, *14*), or secondary ion mass spectrometry (*15*).

[1]Agricultural Biotechnology Research Center, Academia Sinica, Taipei 115, Taiwan.
[2]Advanced Imaging Center, Howard Hughes Medical Institute Janelia Research Campus, Ashburn, VA 20147, USA.
*Corresponding author. Email: zcybele3@sinica.edu.tw

Other ions have been monitored in living tissue through Förster resonance energy transfer (FRET)–based biosensors. FRET sensors are fusion proteins that report on a target molecule through interactions with a sensory domain that cause changes in a protein conformation (*16*). These conformational changes affect the efficiency of energy transfer from a fused FRET donor fluorescent protein to a fused FRET acceptor fluorescent protein. Changes in energy transfer can be detected by measuring changes in the relative intensity of the two fluorescent proteins (ratio change) after excitation of the donor. The ratio change reports target molecule concentration. Here, we report the development of a fluorescent biosensor, NitraMeter3.0, to monitor the dynamics of NO_3^- in plants.

RESULTS AND DISCUSSION

NO_3^- FRET sensor engineering and optimization

The bacterial NasR protein is a soluble receptor that contains a NO_3^- and nitrite (NO_2^-)–sensing domain (NIT), which serves as a NO_3^--binding pocket (*17*–*19*). We generated a biosensor by cloning the NIT domain as a Gateway Entry clone and then recombining it with a previously designed Gateway Destination vector (pDR-FLIP39) that carries an enhanced dimerization (ed) variant of Aphrodite (edAFP), as the FRET acceptor, and of enhanced cyan fluorescent protein (edeCFP), as the FRET donor (*20*). The fusion proteins were expressed in protease-deficient yeast, purified (*20*), and analyzed in a spectrofluorometer for NO_3^--dependent alterations in the fluorescence emission curves after FRET donor excitation (Dx) at 428 nm (fig. S1). Within the NIT domain fusion protein, the fluorophores were within Förster distance, as evidenced by resonance energy transfer; however, NO_3^- addition did not trigger a significant change in the energy transfer rate between the emission at 530 nm [Dx acceptor emission (DxAm)] and the emission at 488 nm [Dx donor emission (DxDm)] that could act as a FRET ratio change sensor (ΔDxAm/DxDm). The initial emission ratio (ΔDxAm/DxDm) of the NIT domain fusion protein was greater than 1.2 (fig. S1). To further optimize the sensor, we tested the effect of replacing the NIT domain with the entire NasR protein (Fig. 1A). The NasR fusion construct showed a NO_3^--triggered increase in emission ratio. The NasR FRET biosensor was named NitraMeter1.0 (NiMet1.0) and reported NO_3^- levels with a positive ratio change (ΔDxAm/DxDm) (fig. S2). Fluorescent protein pair variants and different lengths of
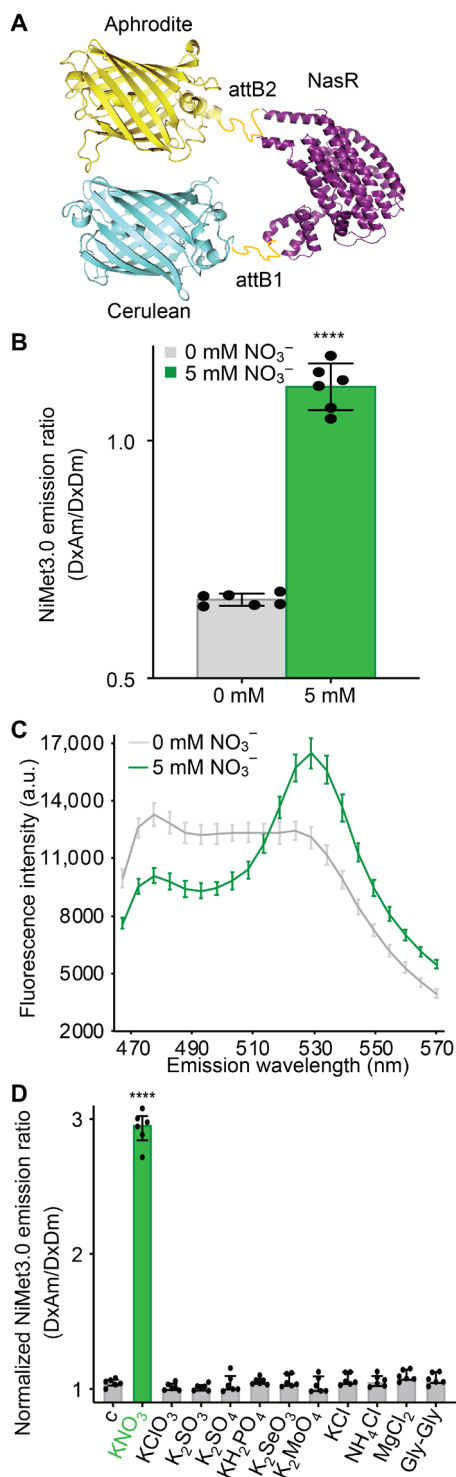
Fig. 1. Engineering and specificity for NO₃⁻ of nitrate biosensor, NiMet 3.0. (**A**) Structural model of NiMet3.0 bound to NO_3^-. NasR, a NO_3^--binding protein, was fused via attB1 and attB2 linkers to a fluorescent protein FRET pair (donor, Aphrodite, and acceptor, Cerulean). The NasR protein (purple) representation is from a published structure of NasR [Protein Data Bank (PDB) 4AKK (*17*)]. The Aphrodite (yellow) representation is from a published structure of Venus [PDB 1MYW (*57*)] and the Cerulean (blue) representation is from a published structure of Cerulean [PDB 2WSO (*58*)]. (**B** and **C**) Fluorescence emission ratio at 530 nm (B) and emission wavelength scan (C) of purified NiMet3.0 protein with and without NO_3^-. The NO_3^- concentration as indicated in the figures. a.u., arbitrary units. (**D**) Substrate specificity of purified NiMet3.0 treated with the indicated compounds at 5 mM concentrations. Only NO_3^- triggered responses that were significantly different from control (c) (****$P < 0.0001$, *t* test). The presented data are means ± SD of six biological repeats. Experiment performed as in (B).

linkers can have marked effects on sensor responses (*21–23*). In an attempt to optimize NiMet1.0, different FRET pairs including brightness variants and truncation variants and different lengths of linkers fused to either the N or C terminus of the Gateway Destination vectors [pDR-FLIP30, pDR-FLIP39, and pDR-FLIP42-linker (*20*)] were tested. A FRET pair variant containing citrine and monomeric Cerulean (mCer) was consistently NO_3^- responsive; we named this biosensor variant NiMet2.0 (fig. S3). NasR with L12 linkers showed a larger NO_3^--triggered response when fused to the citrine/mCer pair (fig. S3). Furthermore, NasR with no L12 linkers sandwiched by Aphrodite t9 (AFPt9) and mCer (pDR-FLIP30) yielded the highest ratio change and the lowest FRET initiation ratio; this variant was thus named NiMet3.0 (Fig. 1B). Considering the crystal structure of NasR (*17*) and our observed DxAm/DxDm values for NiMet3.0 (hereafter referred to as NiMet3.0 emission ratio) with and without NO_3^- (Fig. 1C), we hypothesize that NiMet3.0 switches from a low-FRET to high-FRET average state upon binding to NO_3^-.

Kinetics, pH, selectivity, and nonresponsive NiMet3.0
To test the specificity of NiMet3.0 to NO_3^-, we examined different forms of nitrogen and other anions. Neither other anions nor other nitrogen forms, like ammonium or a peptide, triggered emission ratio changes; thus, the NiMet3.0 sensor is specific to NO_3^- (Fig. 1D). To determine the dynamic range of NO_3^- detection by NiMet3.0, we measured the dissociation constant (K_d) of purified NiMet3.0

in vitro by tracking dose-dependent changes in NiMet3.0 emission ratios for NO_3^- (Fig. 2A). The sensitivity of NasR for NO_3^- is in the micromolar to millimolar range (*19*). The K_d of NiMet3.0 was ~90 μM for NO_3^- and reached a maximum at NO_3^- concentrations above 1 mM (Fig. 2A). This affinity is comparable with the NasR sensitivity for NO_3^-. Nonresponsive variants of NiMet3.0, an important control of NiMet3.0 specificity, were generated via mutation of NasR residues involved in NO_3^- binding (Fig. 2B). NiMet3.0-R49A, NiMet3.0-R50A, NiMet3.0-R176A, and NiMet3.0-R236A carry alanine substitutions in the predicted NO_3^--binding pocket of NasR based on the crystal structure of the NasR protein and have been shown to disrupt NO_3^- responses (*17*). NiMet3.0-R49A and NiMet3.0-R236A still showed detectable response to NO_3^- but with lower emission ratios compared with NiMet3.0, whereas NiMet3.0-R50A and NiMet3.0-R176A, the substitution in the NasR-binding pocket, showed no responses to NO_3^-, likely due to disrupted salt bridges that function in the interaction with NO_3^- (Fig. 2C) (*17*). The above mutant biosensors are evidently nonresponsive to NO_3^- and carry a NO_3^- binding pocket that is predicted to be nonresponsive in planta with endogenous NO_3^-. Together, these data strongly support the hypothesis that NiMet3.0 specifically measures NO_3^- concentrations and can report the dynamics of changes in NO_3^- levels.

To test the specificity of the NiMet3.0 response to NO_3^- in planta, we generated stable transgenic *Arabidopsis* lines expressing either NiMet3.0 or the nonresponsive control NiMet3.0-R176A (under
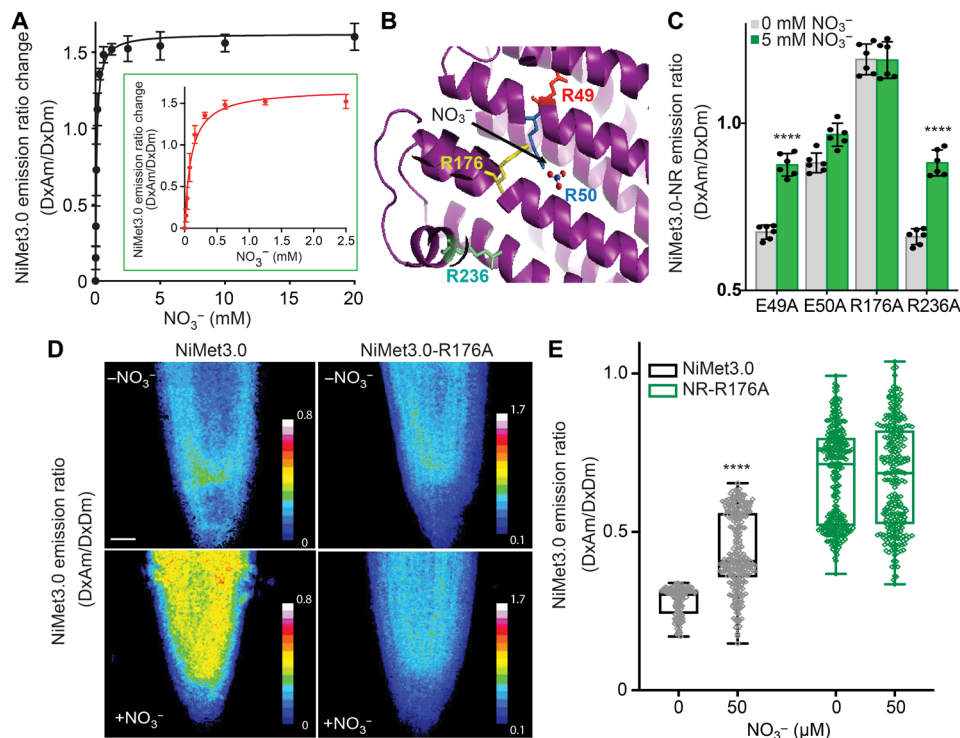

Fig. 2. Fluorescence emission ratio response of purified NiMet3.0 to NO_3^- in vitro and in vivo. (**A**) NiMet3.0 fluorescence response to increasing concentrations of NO_3^-. Inset: Enlargement of the NiMet3.0 fluorescence response from 0 to 2.5 mM NO_3^-. (**B**) NiMet3.0 residues of the NO_3^- binding pocket of NasR mutagenized to make NitMet3.0 nonresponsive constructs (NiMet3.0 NR). Four residues of NasR, R49, R50, R176, and R236 (red, blue, yellow, and green, respectively) were mutagenized to alanine. (**C**) Fluorescence emission ratios of purified NiMet3.0-NR proteins with and without NO_3^- treatment. NO_3^- concentration is as indicated in figures. ****$P < 0.0001$, Student's *t* test. Means ± SD of six biological repeats are presented. (**D**) Images of NiMet3.0 and NiMet3.0 NR-R176A emission ratios of the root tips in 6-day-old seedlings in transgenic Col-0 grown with or without 5 mM NO_3^-. Scale bar, 25 μm. (**E**) Corresponding quantitative analysis of NiMet3.0 emission ratios of root in (D). Beeswarm box plot of NiMet3.0s emission ratios from root region (*n* > 80 areas from three independent seedlings for each genotype of three biological experiments). ****$P < 0.0001$, Student's *t* test. NiMet3.0 emission ratios were statistically different compared to no NO_3^-.

the control of the strong constitutive CaMV35S). The root tips of 6-day-old seedlings from both lines germinated and grown in nitrogen-free medium with exogenous NO_3^- pulses directly to the primary root for 5 min were examined. Transgenic lines expressing NiMet3.0, but not NiMet3.0-R176A, showed significant emission ratio changes to NO_3^- in roots (Fig. 2D; quantification in Fig. 2E), indicating that NiMet3.0 can specifically detect NO_3^- in plants.

For the generation of high-sensitivity FRET sensors, many parameters are critical, such as sensory domain for affinity and specificity, fluorescent proteins for brightness and ligand-induced FRET changes, and linkers for the effect on sensor responses (16, 24, 25). Here, we successfully engineered NiMet1.0 responses to NO_3^- and further optimized the sensor to create NiMet2.0 and NiMet3.0. NiMet3.0 had a bigger emission change ratio, a better signal-to-noise ratio, and a lower initiated ratio by iterative optimization with ligand-binding domains, linkers, and FRET donor and acceptor fluorescent proteins (Fig. 1). Replacing key NO_3^--binding residues in the ligand-binding pocket of NasR with alanine, we generated a nonresponsive sensor of NiMet3.0, which showed no emission ratio changes to NO_3^- pulses (Fig. 2, B and C). Moreover, NiMet3.0 did not respond to a variety of other nitrogen sources and anions, e.g., sulfate, sufite, selenite, or molybdate, or chlorate. Chlorate is structurally similar to NO_3^- as an analog and is an efficient substrate for NO_3^- reductase (Fig. 1D). Thus, the failure of chlorate to trigger NiMet3.0 emission ratio change in vitro was probably caused by the different charge with chlorate being more electronegative then NO_3^- (26) and/or NasR exhibiting considerable selectivity for inducers (17). Corresponding results were shown in the roots of a nonresponsive sensor of a NiMet3.0 transgenic plant; these results support the notion that NiMet3.0 specifically detects NO_3^- in plants (Fig. 2, D and E). The concentration of NO_3^- in plants varies. The cytoplasm is an important compartment for NO_3^- events. When provided with unlimited supplies of NO_3^-, NO_3^- concentrations in the root or shoot can reach up to 100 mM. Most of the NO_3^- is stored in the vacuole (27). The K_d of NiMet3.0 was ~90 µM for NO_3^- (Fig. 2A). In the future, we propose that the parameters outlined above will be suitable for manipulation to engineer sensors with different affinities to NO_3^- detection.

Expression and characterization of nlsNiMet3.0 in planta

It is assumed that NO_3^- and other small molecules/ions readily diffuse between the cytosol and nucleoplasm via nuclear pores; thus, a sensor targeted to the nucleus will allow the analysis of NO_3^- accumulation in the combination of these compartments, which is effectively cytosol. To assess the control of NO_3^- distribution in planta, we generated stable transgenic Arabidopsis lines expressing a nuclear-targeted variant of NiMet3.0 (nlsNiMet3.0) under the control of a promoter fragment previously shown to direct broad expression [p16 (28)]. Expression of nlsNiMet3.0 did not result in detectable phenotypic changes in seedlings or plants (fig. S4). Purified nlsNiMet3.0 showed similar in vitro responses to NO_3^- as NiMet3.0, and exposure to NO_3^- pulses under different pH values from 5.5 to 7.5 had no effect on the emission ratio (figs. S5 and S6A). These data suggest that the nlsNiMet3.0 sensor can be a highly useful tool in studies of plant development and growth. The emission ratio of nlsMiMet3.0 in the apical meristem zone of primary roots, which were grown in nitrogen-free medium for 5 days with NO_3^- addition for 5 min or with NO_3^- addition for 5 min and removal for 15 min, respectively, was examined. When the emission

ratios of primary root cells exposed to NO_3^- pulses were recorded, nlsNiMet3.0 showed a rapid response to NO_3^- pulses, and the signal was reversible when NO_3^- was withheld (Fig. 3A). We further examined the responses of nlsNiMet3.0 in roots to addition of various exogenous concentrations of NO_3^- for 5 min as described above. In roots, the K_d of nlsNiMet3.0 was ~130 µM for NO_3^- (Fig. 3B and fig. S7). This affinity was comparable to the NiMet3.0 affinity for NO_3^- in vitro. It should be noted that the apparent correlation in planta is consistent with signal site binding with saturation, but additional experiments will be needed to define the absolute concentrations. The NasR protein responded equivalently to both NO_3^- and NO_2^- (18). Purified NiMet3.0 in vitro responded to NO_2^- with K_d ~ 2 µM (fig. S6, A and B); however, no significant emission ratio changes were observed in primary root cells exposed to NO_2^- pulses (fig. S6, C and D). These data support the results above, suggesting that NiMet3.0 responds specifically to NO_3^- pulses (Figs. 2D and 3, A and B).

NO_3^- is a significant source of nitrogen for bacteria and plants. NasR-encoding protein, which contains the NIT domain, controls NO_3^- and NO_2^- assimilation in Klebsiella oxytoca (18). NarX is another NO_3^-- and NO_2^--binding protein that controls NO_3^- and NO_2^- respiration in proteobacteria (29). NasR and NarX protein are both highly selective for NO_3^- and NO_2^-, and neither responds to chlorate. Moreover, NarX discriminates efficiently between NO_3^- and NO_2^-, whereas NasR responds equally well to both. Our green fluorescent protein (GFP)–based NiMet3.0 sensors responded to NO_3^- and NO_2^- in vitro; however, with different affinities, K_d ~ 90 µM and K_d ~ 2 µM, respectively (Fig. 2A and fig. S6B). The revealed crystal structure of NasR showed that its NIT domain is structurally similar to the periplasmic input domain of the NarX two-component sensor. Two invariant arginyl residues located on adjacent α helices of the NIT domain are critical for response to NO_3^- (17). How the fused GFPs and linkers in NiMet3.0 affect its affinity to NO_3^- and NO_2^- and whether NarX can be used as a sensory domain for the sensor development to discern between NO_3^- and NO_2^- will need further exploration.

NO_2^- did not trigger a nlsNiMet3.0 emission ratio change in vivo in the root (fig. S6, C and D), although it did in vitro (fig. S6, A and B). NO_2^-, a metabolite of NO_3^- assimilation, is a form of inorganic nitrogen that is widely available in soil and aquatic environments. NO_2^- can be taken up by free diffusion or active transport. Several NO_2^- transporters have been found in unicellular microorganisms and higher plants, e.g., NAR1 in Chlamydomonas (30), CsNitr1-L/S in cucumber (31–33), VvNPF3.2 in grapevine, and AtNPF3.1 in Arabidopsis (34). AtNPF3.1 mainly plays a key role in vascular tissue due to its expression in smaller veins (34). A previous report stated that the Atnar2.1 mutant, lacking a functional high-affinity NO_3^- transport system, is capable of constitutive NO_2^- influx in Arabidopsis, suggesting the existence of a NO_2^--specific transporter in Arabidopsis (35). Thus, our results for NO_2^- on nlsNiMet3.0 in root warrant further investigation of NO_2^- acquirement and distribution in plants under various environmental conditions and genetic analyses, such as different NO_2^- concentrations and Atnar2.1 mutant.

Live-cell imaging of nlsNiMet3.0 response to endogenous and exogenous NO_3^- in roots

To explore whether NiMet3.0 is suitable for measuring NO_3^- distribution in plants, we investigated nlsNiMet3.0 emission ratios around the central section (~1.5 µm) of the apical meristem and the transition zones in the primary root axis of wild-type Col-0, a NO_3^- transporter
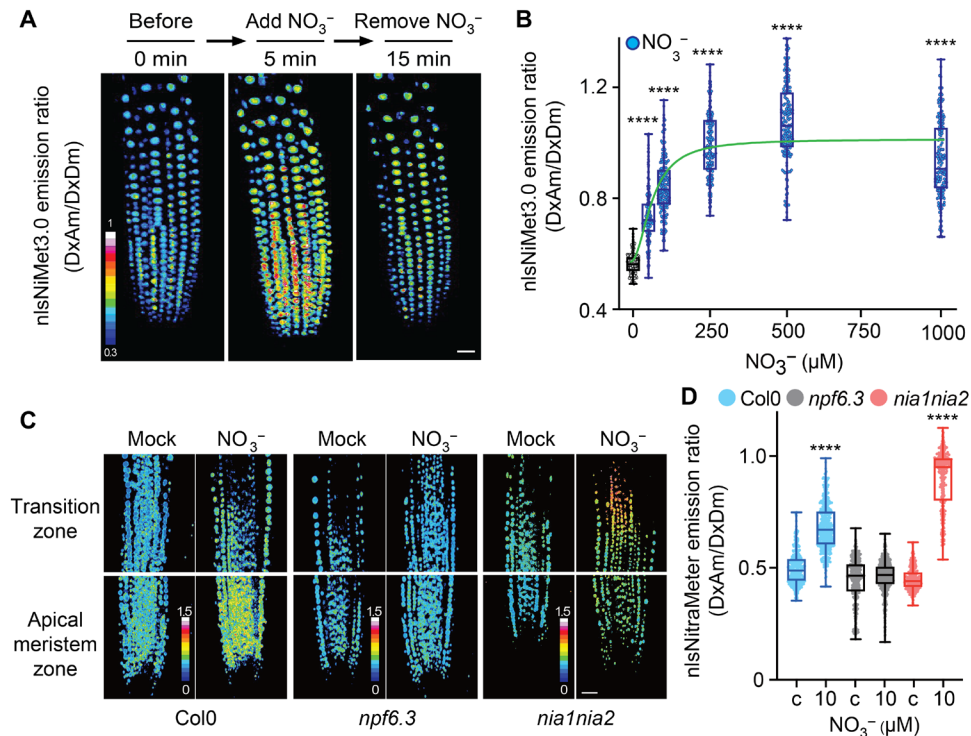
Fig. 3. Emission ratios of nlsNiMet3.0 in root tips before and after NO_3^- treatment in *Arabidopsis* roots. (**A**) Three-dimensional images of nlsNiMet3.0 emission ratios of 5-day-old root meristem zone in transgenic Col-0 before a NO_3^- pulse, after the NO_3^- pulse, and after removing the NO_3^-. NO_3^- (50 μM) was used. Scale bar, 25 μm. (**B**) Beeswarm and box plot of NO_3^- concentration-dependent nlsNiMet3.0 emission ratios for nuclei of root tips from fig. S7. Green line indicates as nonlinear fit of nlsNiMet3.0 K_d curve. ****$P < 0.0001$, Student's *t* test. Means ± SD of three biological repeats are presented. (**C**) Images of nlsNiMet3.0 emission ratios of 6-day-old root zones (meristem and transition zone) in FRET transgenics in wild-type Col-0, *npf6.3*, and *nia1nia2* backgrounds grown with or without NO_3^-. Scale bar, 25 μm. (**D**) Corresponding quantitative analysis of nlsNiMet3.0 emission ratios of root in (C). Beeswarm and box plot of nlsNiMet3.0 emission ratios for nuclei of the central region ($n > 180$ nuclei from three independent seedlings for each genotype of three biological experiments). nlsNiMet3.0 emission ratios were statistically different in *npf6.3* and *nia1nia2* compared to Col-0 backgrounds (c, as mock as control). ****$P < 0.0001$.

mutant [*npf6.3/NTR1;1/chl1-5* (*36*)], and a NO_3^- reductase mutant [*nia1nia2* (*37*)]. Seedlings were germinated and grown on agar plates without (as mock) or with 10 μM of NO_3^- at pH 5.5 and exposed to long days (16-hour light/8-hour dark) for 5 days (Fig. 3C). NO_3^- uptake into root cells requires NO_3^- transporters (*36*). In wild-type roots, we observed an overall higher emission ratio in seedlings grown on NO_3^--containing agar compared with those grown without NO_3^- (nitrogen-free agar plates). There was an apparent gradient of NO_3^- in the root tip, with high nlsNiMet3.0 emission ratios in the apical meristem zone that reduced to lower nlsNiMet3.0 emission ratios in the root transition zone (Fig. 3C), although local variation was observed. As expected, the NO_3^- transporter *npf6.3* mutant plants showed lower nlsNiMet3.0 emission ratios in all root zones with or without NO_3^- in the medium compared to the wild type, supporting the idea that NPF6.3 functions as a major NO_3^- transporter bringing external NO_3^- into roots. Furthermore, there was an overall increase of nlsNiMet3.0 emission ratios with NO_3^- treatment in the root of the *nia1nia2* mutant compared to that in the wild type and higher nlsNiMet3.0 emission ratios in the cortical cells of the transition zone (Fig. 3C), suggesting an area of higher NIA1/NIA2 protein or activity levels in the root. Our findings support the idea that nlsNiMet3.0 is potentially suitable for measuring NO_3^- distribution in planta. Quantification results corresponding to Fig. 3C are shown in Fig. 3D.

To explore which tissue(s) or zone(s) along the root is (are) responsible for NO_3^- uptake, a central section of the Col-0 primary root axis as described above underwent short-term exogenous NO_3^- addition/removal. We analyzed nlsNiMet3.0 emission ratios in roots of *Arabidopsis* seedlings, which were germinated and grown on agar plates at pH 5.5 without nitrogen for 5 days, before NO_3^- pulsing, 5 min after NO_3^- pulsing, and 15 or 30 min after treatment with exogenous NO_3^- during external washout. Similar to the long-term NO_3^- growth results shown in Fig. 3C, overall higher nlsNiMet3.0 emission ratios were rapidly observed in the root meristem zone with exogenous NO_3^- applied for 5 min (Fig. 4A), although the differential nlsNiMet3.0 emission ratios across the root may result from the competing processes of influx, efflux, xylem and vascular loading, and NO_3^- reduction. Exogenous treatment of *Arabidopsis* roots with NO_3^- did not increase nlsNiMet3.0 emission ratios in the endodermis cells, whereas it triggered increased nlsNiMet3.0 emission ratios in the epidermis, pericycle, and stele cells, with highest ratios seen in the cortex cells (Fig. 4B). After washing out the exogenous NO_3^-, the increased nlsNiMet3.0 emission ratio was rapidly reduced in all root cells. After washout, the cortex cells in the root meristem maintained relatively high levels of NO_3^- (Fig. 4, A and B). It should be noted that, after accumulation of exogenous NO_3^-, nlsNiMet3.0 was able to report the depletion of NO_3^- from all types of cells of the roots (Figs. 3A and 4, A and B).
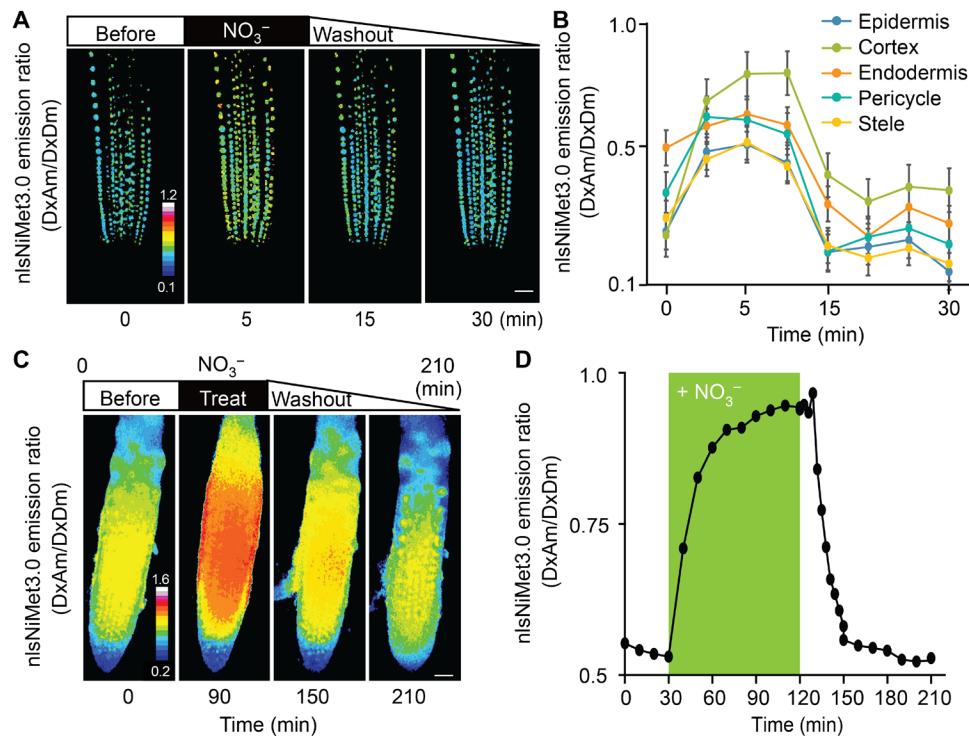
Fig. 4. Emission ratios of nlsNiMet3.0 in roots under time-course treatment with NO_3^-. (**A** and **B**) Images and corresponding quantitative analysis of *Arabidopsis* root meristem zone before and after NO_3^- treatment. Images obtained after incubation with 50 μM NO_3^- for 5 min. Images were taken before or immediately after NO_3^- treatment for 5 min or during the washout at 15 and 30 min. Scale bar, 25 μm. (B) Quantitative analysis of nlsNiMet3.0 emission ratios for nuclei of epidermis, endodermis, cortex, pericycle, and stele cells in roots from (A). Complete experiments were repeated at least three times with similar results. (**C**) Time-course treatment of nlsNiMet3.0 with NO_3^- in root meristem zone. Images were taken before or immediately after NO_3^- treatment for 90 min or during the washout at 150 and 210 min. Scale bar, 25 μm. (**D**) Corresponding quantitative analysis of nlsNiMet3.0 emission ratios of root in (C). Complete experiments were repeated at least three times with similar results.

The accumulation of exogenously applied NO_3^-, detected by nlsNiMet3.0 in the nuclei of root cells, reflects an accumulation of NO_3^- in the cytosol/nucleoplasm and a balance of NO_3^- net flux between import and depletion activities, for example, metabolism, export, and compartmentation. To quantify this cooperative activity with high spatiotemporal resolution, we performed time-course experiments on *Arabidopsis* roots using light-sheet microscopy, a microfluidic device that allows imaging of roots growing in fluorinated ethylene propylene (FEP) tubes with a perfusion control system (fig. S8). *Arabidopsis* seedlings were germinated and grown in $^1/_{20}$ strength Murashige Skoog (MS) medium at pH 5.5 for 5 to 6 days and then perfused with the medium without nitrogen for another 1 to 2 days. After 90 min of perfusion with 10 μM of NO_3^-, the nlsNiMet3.0 emission ratio in the meristem zone of the primary root was nearly saturated, indicating a dynamic balance of NO_3^- net flux in the roots or concentrations of NO_3^- in cytosol/nucleoplasm over the capacity of nlsNiMet3.0 (Fig. 4, C and D). With washout, the emission ratio rapidly reduced back to the initial levels (Fig. 4, C and D, and movie S1). These results also indicated that the steady-state concentrations in the cytosol/nucleoplasm were achieved in 90 min of perfusion with 10 μM of NO_3^-.

Investigation of nutrient acquisition has relied heavily on techniques that integrate uptake over the entire root system. Unfortunately, this approach fails to reveal which regions of the root are actually involved in the uptake process. The localization of uptake along the root axis correlates with root development, structure, metabolism, and transport processes. It is also reasonable to expect that cellular biochemistry and metabolic requirements may also vary with the position along the root axis. Net fluxes of NO_3^- into the roots vary both with position along the root axis and with time. These variations may not be consistent in different plants, in which different roots show different temporal and spatial patterns of uptake (*12*) and NO_3^- activity (*38*). Our new genetically encoded fluorescent sensor, NitraMeter (NiMet), that monitors the net NO_3^- fluxes in real time in the cellular or subcellular compartments with high spatiotemporal resolution in a minimally invasive manner in living cells provides a solution and enables determination of uptake of NO_3^-, steady-state net NO_3^- fluxes, and NO_3^- dynamics in the cytosol/nucleoplasm in roots with high spatial and temporal resolution. When exogenous NO_3^- is pulsed to roots, a rapidly increased emission ratio of NiMet3.0 in Col-0 suggests the high accumulation of NO_3^- in Col-0 root (Figs. 2, D and E, 3, A and B, and 4). This is possibly due to the higher rate of NO_3^- uptake activity by transporter as the seedlings were grown under no- or low-nitrogen conditions. The higher emission ratio in the meristematic zone of primary root in Col-0 suggests that the meristematic zone is mainly responsible for uptake of external NO_3^- into the root. Many NO_3^- transporters dominantly expressed in the primary root have been identified and functionally characterized in the past (*36*). The results of the responses of nlsNiMet3.0 in *npf6.3* mutant (Fig. 3, C and D)

also support the function of NPF6.3 as a major NO_3^- transporter in primary root (*39*) even under different growth conditions. Moreover, the higher and faster emission ratio in root cortex cells compared to all other cells after exposure to NO_3^- (Fig. 4, A and B) suggests a higher rate of NO_3^- uptake and/or transport. The endodermis cells in the root showed a relatively high NO_3^- accumulation compared to all other cells when seedlings were grown under nitrogen-free conditions (0 min; Fig. 4B); meanwhile, the level of NO_3^- accumulation after exposure to exogenous NO_3^- pulses increased slowly. These data suggest that NO_3^- accumulation in the endodermis cells in the primary root may play an important role as a NO_3^- hub for the plant to respond and adapt to various environments accordingly. AtNPF1.3, which is highly expressed in the endodermis cells in the root, has recently been demonstrated to be a NO_3^- transporter in vitro (*40*). It is also known that NO_3^- is a potent signaling molecule that regulates global gene expression and many physiological processes, such as root architecture and flowering (*1*). The cross-talk among NO_3^- accumulation and NO_3^- signals in response to nitrogen availability changes in different cell types in the root, especially in the endodermis cells, will need further investigation.

In addition, a higher emission ratio was observed in the transition zone of *nia1nia2* root, suggesting that the NO_3^- reductase levels or activity is higher. NO_3^- reductase is the key enzyme responsible for NO_3^--to-NO_2^- reduction in plant cells (*41*). In *nia1nia2* mutant, higher emission ratios of nlsNiMet3.0 in roots indicated higher accumulation of NO_3^- (Fig. 3, C and D), supporting the idea that a comparison of uptake rates for wild-type and *nia1nia2* roots would provide insight into rates of net flux of NO_3^-. Many studies have shown that the amount of NO_3^- activity is not what limits its activity in cells. NO_3^- reductase is known to be under complex regulation both at the transcriptional level by the application of NO_3^- and at the posttranscriptional level by environmental conditions, such as light, dark, anoxia, hormones, and pH (*42–44*). Moreover, NO_3^- reductase activity affects the cytosolic NO_3^- pools in plants under different environmental conditions (*44*). In the past, many results have demonstrated longitudinal gradients in respiratory activity and NO_3^- assimilatory enzyme activity (*45–47*). Notwithstanding, the expression of NO_3^- reductases is regulated by various factors, resulting in a diurnally differential expression pattern; thus, a comparison of uptake rates and investigation of whether/how NO_2^- effects nlsNiMet3.0 in wild-type and *nia1nia2* mutant roots would provide insight into the rates of uptake and subsequent reduction. Furthermore, whether the remaining activity is attributed to vacuolar sequestration will need further exploration.

To be incorporated into amino acids, once NO_3^- is taken into cells by transporters, NO_3^- is reduced to NO_2^- in the cytosol (pH ~ 7.5) by NO_3^- reductase, and then, NO_2^- is reduced to NH_4^+ in the plasmids or chloroplasts (pH ~7 to 8) by a NO_2^- reductase. NO_3^- can also be transported into vacuoles (pH ~5 to 7) for storage or transported to the shoot by the xylem (pH ~5 to 6) or phloem (pH ~7 to 9). In animals, including humans, NO_3^- and NO_2^- are recognized as being inert oxidants of nitric oxide, which is a key signaling factor in physiology including vascular homeostasis, neurotransmission, and host defense (*24, 48*). As nlsNiMet3.0 was found to be less sensitive to pH between 5.5 to 7.5 in vitro, nlsNiMet3.0 could potentially be applied to a wide variety of living cells and organisms including plants and animals to provide insights into NO_3^- dynamics.

GFP-based sensors enable monitoring of flux into intact cells. However, to generate a detailed flux model, further information will be required such as the nature and kinetics of the contributing transporters as well as the contribution of vacuoles. NO_3^- transporters, which have been intensively studied in the past decades in plants (*36*), are placed in strategic positions to control how much NO_3^- can enter a given cell at a given point in time; however, it is still difficult to know where the modifications take place and to determine the effect of each step of transportation. Recently, ratiometric fluorescent NO_3^- sensors for activity of NO_3^- transporters named NiTrac1 and NiTrac-NPF1.3 have been reported to be able to track the movement of NO_3^- through the cell membrane (*40, 49*). Here, we report NitraMeter3.0 sensor (NiMet3.0) as a new and highly useful tool that can be used in living plant roots to quantify NO_3^- concentrations and dynamics (fig. S9). In the future, it is hoped to test *Arabidopsis* mutant lines for NO_3^- reductase and various transporters expressing NiTrac1, NiTrac-NPF1.3, and NiMet3.0 sensors in the roots.

MATERIALS AND METHODS
DNA constructs
The construction of the sensor expression vector has been described (*50*). Constructs were inserted by Gateway LR reactions into the yeast expression vectors pDRFlip30, pDRFlip39, pDRFlip42-linker, and pDRFlip-GW (Gateway). The pDRFlip30 vector sandwiches the insert between an N-terminal AFPt9 variant (*25*), with nine amino acids truncated off the C terminus, and a C-terminal mCer (*51*). pDRFlip39 sandwiches the inserted polypeptide between an N-terminal enhanced dimer Aphrodite t9 (edAFPt9) and C-terminal fluorescent protein enhanced dimer, with seven amino acids and nine amino acids truncated from the N terminus and the C terminus of eCyan (t7.ed.eCFPt9), respectively. pDRFlip42-linker carries an N-terminal citrine and a C-terminal mCer (*51*). The pDRFlip42 vector was digested with Kpn I (New England Biolabs) for insertion of additional linker sequences (Arg-Ser-Arg-Pro-Thr-Arg-Pro-Gly-Glu-Leu-Gly-Thr) to generate the pDRFlip42-linker vector. The full-length open reading frame of NasR, the NIT domain of NasR, or NasR carrying point mutations from *K. oxytoca* (*17*) in the pDONR221 Gateway Entry vector was used as sensory domains for creating the NO_3^- sensors NiMet-NIT, NiMet1.0, NiMet2.0, NiMet3.0, nlsNiMet3.0, or NiMet3.0-NRs. The yeast expression vectors were then created by Gateway LR reactions between different forms of pDONR221-NasR/NIT and different pDRFlip-GWs, following the manufacturer's instructions.

Generation of NiMet3.0-NR mutants
The NO_3^- binding domain of the NasR Entry clone for NiMet3.0 was altered using the QuikChange Lightning Site-Directed Mutagenesis Kit (Agilent Technologies) according to the manufacturer's instructions to generate the NiMet3.0-NR mutations. Primers for site-directed mutagenesis of NiMet3.0 to create NiMet3.0-NR were as follows: R49A, 5′-catatgctgcagtgtgcacggggagccagtaat-3′ (forward) and 5′-attactggctccccgtgcacactgcagcatatg-3′ (reverse); R50A, 5′-gtacatatgctgcagtgtgaagcgggagccagtaatatctg-3′ (forward) and 5′-cagatattactggctcccgcttcacactgcagcatatgtac-3′ (reverse); R176A, 5′-cgcgggtcaggcacgggcgctgg-3′ (forward) and 5′-ccagcgcccgt-gcctgacccgcg-3′ (reverse); and R236A, 5′-gagattgagcagctggctcgtgtc-gcttgcac-3′ (forward) and 5′-gtgcaagcgacacgagccagctgctcaatctc-3′ (reverse).

Expression of sensors in yeast

A *Saccharomyces cerevisiae* strain BJ5465 [American Type Culture Collection, 208289 (*MATa ura3-52 trp1 leu2-Δ1 his3-Δ200 pep4* ::*HIS3 prb1-Δ1.6 R can1 GAL*] (*52*), obtained from the Yeast Genetic Stock Center (University of California, Berkeley, CA), was transformed with pDRFlips yeast expression plasmids using a lithium acetate transformation protocol (*53*). Transformed yeast was selected on solid yeast nitrogen base (YNB; minimal yeast medium without nitrogen; Difco) supplemented with 2% glucose and –ura dropout medium (Clontech). Single colonies were grown in 5 ml of liquid YNB supplemented with 2% glucose and –ura dropout under agitation (230 rpm) at 28°C until optical density at 600 nm ~ 0.8 was reached for fluorescence analysis of sensor expression and for metal affinity chromatography purification of sensors. Yeast strains expressing sensors were grown in 30-ml cultures in –ura dropout medium in 50-ml culture tubes.

Fluorescence analysis of purified sensors

Biosensors were purified by metal affinity chromatography. Yeast lysates were diluted 1:2 in 50 mM Mops and 10 mM imidazole (pH 7.4) and then filtered through a 0.45-μm polyethersulfone (PES) filter and bound to Poly-Prep chromatography columns (Bio-Rad) containing His-Pur Cobalt resin (Bio-Rad). Columns were then washed twice with 50 mM Mops and 10 mM imidazole (pH 7.4) and eluted in 50 mM Mops and 150 mM imidazole (pH 7.4). Samples were diluted in 50 mM Mops (pH 7.4). Fluorescence was measured in a fluorescence plate reader (M1000, Tecan, Austria), in bottom-reading mode using a 7.5-nm bandwidth for both excitation and emission (*54*, *55*). Typically, emission spectra were recorded (λ_{em}, 470 to 570 nm; step size, 5 nm). To quantify fluorescence responses of the sensors to substrate addition, 100 μl of substrate [dissolved in 50 mM Mops buffer (pH 5.5, 6.5, or 7.4)] was added to 100 μl of cells in 96-well flat-bottom plates (no. 655101, Greiner, Monroe, NC). Fluorescence from pDRFlip30 (donor, mCer), pDRFlip39 (donor, t7.ed.eCFPp9), and pDRFlip42-linker (donor, mCer) was measured by excitation at λ_{exc} of 428 nm. Determination of the apparent K_d of NiMet3.0 for NO_3^- was performed as described previously (*17*). The purified NiMet3.0 protein was pretreated with 0 to 20 mM NO_3^- or 0 to 0.3 mM NO_2^-. Data are reported as mean and SD of three to four replicates, and each experiment was performed at least three times with similar results. After 15 min, buffer was exchanged to 50 mM Mops (pH 7.4), and fluorescence was analyzed. The emission ratio was subsequently calculated dividing the value of the 530 nm by 488 nm range.

Expression of NiMet3.0, NiMet3.0-NR-R176A, and nlsNiMet3.0 in *Arabidopsis*

The p16 promoter (*28*) from the AT3G60245 gene encoding a 16*S* ribosomal subunit was used to drive the nuclear-localized NiMet3.0 fusion biosensor, whereas the CaMV35S promoter (*56*) was used to drive the NiMet3.0 and NiMet3.0-NR-R176A fusion biosensor in plants. The following construct was inserted into the multiple cloning site of the p16-Kan vector (*20*): 5′-, a sequence coding for the SV40-derived nuclear localization signal LQPKKKRKVGG (*28*), a sequence coding for Aphrodite; a Gateway cassette including *att*R1, Chloramphenicol resistance gene, *ccd*B terminator gene, and *att*R2; a sequence coding for mCer; and a sequence coding for the cMyc epitope tag -3′, or pZPFlip *UBQ10*-KAN vector under control of the *UBQ10* promoter. The resulting Gateway Destination vectors

(p16-FLIPnls30 and pZPFlip30) were then recombined in Gateway LR reactions with NasR or NasR-NR-R176A Entry clones, resulting in NiMet3.0, NiMet3.0-NR-R176A, and nlsNiMet3.0 expression clones. Transgenic plant lines were generated using the *Agrobacterium* floral dip method as described previously (*25*). Transformants were selected on agar plates containing $^1/_2$ strength MS medium with vitamins (PhytoTech Labs, M519) and with kanamycin.

Fluorescence microscopy

Arabidopsis seedlings were either germinated and grown vertically on $^1/_2$ strength MS agar medium ($^1/_2$ strength MS salts without nitrogen; PhytoTech Labs, M531), 1% agar, and 0.05% (w/v) sucrose (pH 5.7) plates or germinated on hydroponic medium solidified with 1% agar (Becton Dickinson Biosciences) within cut pipette tips, 5 mm in length and 1 mm in diameter, that were positioned in an upright position onto a plate with solidified medium for confocal images or light-sheet images, respectively. Plates were stratified for 3 days at 4°C in the dark before being placed in a growth chamber under long-day growth conditions (16-hour light/8-hour dark cycling, temperature cycling of 22°C day/18°C night, 67% relative humidity). For confocal images, 5- or 6-day-old seedlings were placed in solution containing $^1/_2$ strength MS medium [$^1/_2$ strength MS salts without nitrogen and 0.05% sucrose (pH 5.7)] and prepared for imaging on glass slides. Seedlings for light-sheet microscopy were grown for 3 days in the growth chamber, at which time the root tips had almost reached the lower tip outlet. The tips were plugged into a ~3-cm piece of FEP tubing with an inner diameter of 0.115 cm, an outer diameter of 0.195 cm, and wall thickness of 0.04 cm (TEF-CAP, AWG17SW-FEP) and sterilized in 70% ethanol. A closed cultivation system within FEP tubing was used for imaging. Both upper and lower FEP tubes were sealed using gaskets. An inlet and outlet tube were inserted into each side of the gaskets and connected to silicon tubing within a pumping perfusion system. To maintain the humidity within the closed cultivation system, the inner sides of the tubing holder had surrounding water reservoirs. Upon transfer to the light-sheet microscope, the seedling was illuminated by a light connected to a timer switch to maintain the light/dark period. The FEP tubing was filled with $^1/_{20}$ strength MS hydroponic medium (PhytoTech Labs, M519) and incubated for another 3 to 4 days. The FEP tubing was then fixed in a metal holder and placed into the light-sheet microscope chamber, which was filled with water. The $^1/_2$ strength MS salts hydroponic medium without nitrogen (pH 5.5) (PhytoTech Labs, M531) was then continually replaced using a peristaltic pump (GE Healthcare) with a flow rate of 1 ml/hour for another 1 to 2 days before the treatments. The temperature of the microscopy chamber was set at 22°C.

For NO_3^- treatments on glass slides for confocal microscopy (Figs. 2D, 3, A and C, and 4A and figs. S6 and S7C), seedlings were placed on glass slides with 50 μl of solution and surrounded with a rectangle of vacuum grease and covered with a square coverslip equal in height and half the width of the vacuum grease rectangle. The NO_3^- treatment solution could then be exchanged beneath the coverslip by addition to the left and removal from the right side of the coverslip. Images were acquired at the time points indicated in each figure. Three-dimensional images half the diameter of the primary root axis in *Arabidopsis* were acquired and analyzed before and after treatments at the time points indicated in the figures or legends (Figs. 2D, 3A, and 4, C and D, and figs. S6 and S7C). The central layer image of the primary root axis in plants was acquired

(Figs. 3C and 4A) for the analysis of different cell types (epidermis, cortex, endodermis, pericycle, and stele). Images mainly focusing on the primary root tip or the primary root of the apical meristem zone were acquired, as shown in Figs. 2D, 3A, and 4 and figs. S6 and S7. Images collected partially from the apical meristem zone and transition zone in the primary root were acquired and analyzed as shown in Fig. 3 (C and D).

Confocal images were acquired on a Zeiss 780 laser scanning microscope using a 20×/0.8 Plan-Apochromat dry objective or 40×/1.2 C-Apochromat water objective. CFP (440 nm) and yellow fluorescent protein (YFP; 514 nm) were excited with lasers. Fluorescence emission was detected by a GaAsP photomultiplier tube (PMT) detector, set to detect 463 to 508 nm for CFP, and a normal PMT detector, set to 520 to 585 nm for YFP. The laser power was set between 0.5 and 2% with detector gain set to 700 to 750 to image CFP or YFP.

The laboratory-established light-sheet system was made in cooperation with Microlambda Pte Ltd. (Singapore) (fig. S8). Light-sheet imaging (Fig. 4C and movie S1) was performed using a 20× 0.5 dipping objective, two illumination arms with galvanometer scanners, 10× long–working distance objectives, and 445-nm and 515-nm lasers that were used for excitation of CFP and YFP, respectively. For FRET measurements, sequential imaging of CFP and YFP was performed with a DC filter wheel with ET470/24m and an ET535/50m emission filters, driven by a MAC6000 controller (Ludl Electronic Products, Hawthorne, NY). Fluorescence emission was detected by a Hamamatsu Flash 4.0 V3 camera. Imaging data were acquired using MetaMorph software (Downingtown, PA). Data were taken as time series with simultaneous acquisition of FRET donor and acceptor fluorophores under Dx, followed by acquisition of donor and acceptor under acceptor excitation.

Image processing and analysis
Image processing and fluorescence pixel intensity were quantified using Fiji software (http://fiji.sc/). Mean gray values of regions of interest (ROIs) within the root meristem region were calculated as follows: Background was subtracted from all measured intensities as generated ROIs where there was no plant material. Mean intensity values were measured in all four channels (Dx/Dm, Dx/Am, Ax/Dm, and Ax/Am), and that intensity was subtracted from the entire image. Ratio images (DxAm/DxDm) were created using the Ratio Plus plug-in for ImageJ (P. Magalhães, University of Padua, Italy). ROIs were selected and analyzed with the help of the ROI manager tool.

In this work, we presented data using beeswarm and box plots of raw data. In the beeswarm and box plot graphs, the central rectangle spans the first quartile to the third quartile, while the line inside the rectangle shows the median. The whiskers denote 1.5 interquartile ranges from the box, and outlying values were plotted beyond the whiskers. All the statistical analyses were performed using GraphPad Prism version 9.0.0 for Mac (www.graphpad.com).

REFERENCES AND NOTES
1. C. Masclaux-Daubresse, F. Daniel-Vedele, J. Dechorgnat, F. Chardon, L. Gaufichon, A. Suzuki, Nitrogen uptake, assimilation and remobilization in plants: Challenges for sustainable and productive agriculture. *Ann. Bot.* **105**, 1141–1157 (2010).

2. N. M. Crawford, B. G. Forde, Molecular and developmental biology of inorganic nitrogen nutrition. *Arabidopsis Book* **1**, e0011 (2002).

3. A. J. Karley, R. A. Leigh, D. Sanders, Where do all the ions go? The cellular basis of differential ion accumulation in leaf cells. *Trends Plant Sci.* **5**, 465–470 (2000).

4. R. G. Zhen, H. W. Koyro, R. A. Leigh, A. D. Tomos, A. J. Miller, Compartmental nitrate concentrations in barley root cells measured with nitrate-selective microelectrodes and by single-cell sap sampling. *Planta* **185**, 356–361 (1991).

5. H. Zhang, A. Jennings, P. W. Barlow, B. G. Forde, Dual pathways for regulation of root branching by nitrate. *Proc. Natl. Acad. Sci. U.S.A.* **96**, 6529–6534 (1999).

6. P. M. Palenchar, A. Kouranov, L. V. Lejay, G. M. Coruzzi, Genome-wide patterns of carbon and nitrogen regulation of gene expression validate the combined carbon and nitrogen (CN)-signaling hypothesis in plants. *Genome Biol.* **5**, R91 (2004).

7. M. Stitt, Nitrate regulation of metabolism and growth. *Curr. Opin. Plant Biol.* **2**, 178–186 (1999).

8. D. T. Clarkson, A. Gojon, L. R. Saker, P. K. Wiersema, J. V. Purves, P. Tillard, G. M. Arnold, A. J. M. Paans, W. Vaalburg, I. Stulen, Nitrate and ammonium influxes in soybean (*Glycine max*) roots: Direct comparison of ^{13}N and ^{15}N tracing. *Plant Cell Environ.* **19**, 859–868 (1996).

9. M. Y. Wang, M. Y. Siddiqi, T. J. Ruth, A. D. M. Glass, Ammonium uptake by rice roots (II. kinetics of $^{13}NH_4^+$ influx across the plasmalemma). *Plant Physiol.* **103**, 1259–1267 (1993).

10. I. Guevara, J. Iwanejko, A. Dembińska-Kieć, J. Pankiewicz, A. Wanat, P. Anna, I. Gołąbek, S. Bartuś, M. Malczewska-Malec, A. Szczudlik, Determination of nitrite/nitrate in human biological material by the simple Griess reaction. *Clin. Chim. Acta* **274**, 177–188 (1998).

11. G. H. Henriksen, A. J. Bloom, R. M. Spanswick, Measurement of net fluxes of ammonium and nitrate at the surface of barley roots using ion-selective microelectrodes. *Plant Physiol.* **93**, 271–280 (1990).

12. G. H. Henriksen, D. R. Raman, L. P. Walker, R. M. Spanswick, Measurement of Net fluxes of ammonium and nitrate at the surface of barley roots using ion-selective microelectrodes : II. Patterns of uptake along the root axis and evaluation of the microelectrode flux estimation technique. *Plant Physiol.* **99**, 734–747 (1992).

13. S. Kiyomiya, H. Nakanishi, H. Uchida, A. Tsuji, S. Nishiyama, M. Futatsubashi, H. Tsukada, N. S. Ishioka, S. Watanabe, T. Ito, C. Mizuniwa, A. Osa, S. Matsuhashi, S. Hashimoto, T. Sekine, S. Mori, Real time visualization of ^{13}N-translocation in rice under different environmental conditions using positron emitting tracer imaging system. *Plant Physiol.* **125**, 1743–1753 (2001).

14. H. Matsunami, Y. Arima, K. Watanabe, N. S. Ishioka, S. Watanabe, A. Osa, T. Sekine, H. Uchida, A. Tsuji, S. Matsuhashi, T. Itoh, T. Kume, ^{13}N-nitrate uptake sites and rhizobium-infectible region in a single root of common bean and soybean. *Soil Sci. Plant Nutrit.* **45**, 955–962 (1999).

15. P. L. Clode, M. R. Kilburn, D. L. Jones, E. A. Stockdale, J. B. Cliff III, A. M. Herrmann, D. V. Murphy, *In situ* mapping of nutrient uptake in the rhizosphere using nanoscale secondary ion mass spectrometry. *Plant Physiol.* **151**, 1751–1757 (2009).

16. S. Okumoto, A. Jones, W. B. Frommer, Quantitative imaging with fluorescent biosensors. *Annu. Rev. Plant Biol.* **63**, 663–706 (2012).

17. M. Boudes, N. Lazar, M. Graille, D. Durand, T. A. Gaidenko, V. Stewart, H. van Tilbeurgh, The structure of the NasR transcription antiterminator reveals a one-component system with a NIT nitrate receptor coupled to an ANTAR RNA-binding effector. *Mol. Microbiol.* **85**, 431–444 (2012).

18. W. H. Chai, V. Stewart, NasR, a novel RNA-binding protein, mediates nitrate-responsive transcription antitermination of the *Klebsiella oxytoca* M5al *nasF* operon leader *in vitro*. *J. Mol. Biol.* **283**, 339–351 (1998).

19. J. R. Goodson, C. Zhang, D. Trettel, H. E. Ailinger, P. E. Lee, C. M. Spirito, W. C. Winkler, An autoinhibitory mechanism controls RNA-binding activity of the nitrate-sensing protein NasR. *Mol. Microbiol.* **114**, 348–360 (2020).

20. A. M. Jones, J. Å. H. Danielson, S. N. ManojKumar, V. Lanquar, G. Grossmann, W. B. Frommer, Abscisic acid dynamics in roots detected with genetically encoded FRET sensors. *eLife* **3**, e01741 (2014).

21. K. Deuschle, S. Okumoto, M. Fehr, L. L. Looger, L. Kozhukh, W. B. Frommer, Construction and optimization of a family of genetically encoded metabolite sensors by semirational protein engineering. *Protein Sci.* **14**, 2304–2314 (2005).

22. S. A. Hires, Y. Zhu, R. Y. Tsien, Optical measurement of synaptic glutamate spillover and reuptake by linker optimized glutamate-sensitive fluorescent reporters. *Proc. Natl. Acad. Sci. U.S.A.* **105**, 4411–4416 (2008).

23. H. Takanaga, B. Chaudhuri, W. B. Frommer, GLUT1 and GLUT9 as major contributors to glucose influx in HepG2 cells identified by a high sensitivity intramolecular FRET glucose sensor. *Biochim. Biophys. Acta* **1778**, 1091–1099 (2008).

24. C. Nathan, Nitric-oxide as a secretory product of mammalian-cells. *FASEB J.* **6**, 3051–3064 (1992).

25. K. Deuschle, B. Chaudhuri, S. Okumoto, I. Lager, S. Lalonde, W. B. Frommer, Rapid metabolism of glucose detected with FRET glucose nanosensors in epidermal cells and intact roots of *Arabidopsis* RNA-silencing mutants. *Plant Cell* **18**, 2314–2325 (2006).

26. M. T. Madigan, J. M. Martinko, J. Parker, *Brock Biology of Microorganisms* (Prentice Hall, 2000).

SCIENCE ADVANCES | RESEARCH RESOURCE

SCIENCE ADVANCES | RESEARCH RESOURCE